

Calculation of Notch H-Integrals Using Image Correlation Experiments

S.H. Ju

Received: 14 October 2008 / Accepted: 26 May 2009 / Published online: 25 June 2009
© Society for Experimental Mechanics 2009

Abstract This study evaluated notch H-integrals as well as stress intensity factors (SIFs) using image-correlation experiments for anisotropic materials. First, complex displacement and stress functions are deduced into an H-integral equation. Displacements and stresses from image-correlation experiments are then substituted into the H-integral equation to evaluate the notch SIFs. Experimental results compared with finite element analyses show that the SIFs evaluated using the current method are acceptably accurate.

Keywords Composite · Finite element method · H-integral · Image-correlation experiment · Notch stress intensity factor

Introduction

In the past several years, experimental methods have been used to find the stress intensity factors (SIFs) of composites; however, most of them have focused on cracks and notches. The evaluation of notch SIFs is important for engineering, since cracks are often initiated at this location. In the literature review, we focused on the experimental calculation of notch SIFs for anisotropic or bi-materials.

Della and Smith (1998) reviewed some recent developments in superposition methods for calculating linear elastic SIFs and eigenvalues for cracks and notches [1]. Potti et al. (2001) used an empirical relationship between the failure stress and SIFs at failure to examine the fracture strength of thick graphite/epoxy laminates containing surface notches [2]. Niu et al. (2001) did a test with a stainless steel specimen using a Moire interferometry method to confirm the results of the elastic-plastic numerical method [3]. Kondo et al. (2001) used the simple strain gauge method to determine the SIFs of sharp-notched strips based on the two-dimensional theory of elasticity [4]. Mattoni and Zok (2003) determined the SIFs of a single edge-notched porous composite using measured crack mouth opening displacements [5]. Kumagai and Shindo (2004) described an experimental and analytical study on the cryogenic fracture behavior of CFRP-woven laminates under tension with a sharp notch [6]. Xu et al. (2004) studied the fracture characterization of a V-notch tip in PMMA material by means of an optical caustics method [7]. El-Hajjar and Haj-Ali (2005) determined the mode-I fracture toughness of a fiber reinforced composite using the eccentrically loaded, single-edge-notch tension specimen [8]. Yao et al. (2006) used the coherent gradient sensing to study the local deformation field and fracture characterization of mode I V-notch tip, and the SIFs of three-point-bending specimens were calculated [9].

In this study, a Lagrange element is used to smooth the internal displacements and to calculate the boundary displacements from image correlation experiments. Then, the notch SIFs are determined using H-integrals and experimental data. Finally, finite element analyses are used to validate the current method.

S.H. Ju (✉)
Department of Civil Engineering,
National Cheng-Kung University,
Tainan City, Taiwan, Republic of China
e-mail: juju@mail.ncku.edu.tw

In-Plane Displacement and Stress Fields of Notches for Composite Materials

The in-plane isothermal strain-stress relationship for composite materials is

$$\begin{Bmatrix} \varepsilon_x \\ \varepsilon_y \\ \gamma_{xy} \end{Bmatrix} = \begin{bmatrix} a_{11} & a_{12} & a_{16} \\ a_{12} & a_{22} & a_{26} \\ a_{16} & a_{26} & a_{66} \end{bmatrix} \begin{Bmatrix} \sigma_x \\ \sigma_y \\ \tau_{xy} \end{Bmatrix} \quad \text{or} \quad \{\varepsilon\} = [a]\{\sigma\} \quad (1)$$

where $\{\varepsilon\}$, $[a]$, and $\{\sigma\}$ are the strain vector, compliance matrix, and stress vector, respectively. Components a_{ij} are the elements of the compliance matrix that is dependent on material properties, and a_{16} and a_{26} are zero for the orthotropic material whose material symmetry is along axes x and y . In this study, the x - y axes are defined as the notch coordinates in Fig. 1, where the origin is located at the notch tip and the notch center is in the negative x axis, r and θ are the polar coordinates, axes 1 and 2 are the directions of in-plane material symmetry, $+\alpha$ and $-\alpha$ are the angles from the x -axis to notch surfaces counter-clockwise and clockwise, respectively, and angle γ is $2(\pi-\alpha)$. For two-dimensional (2D) anisotropic problems, Lekhnitskii (1963) showed that the displacement and stress are the functions of z_1 , z_2 , p_1 , and p_2 , [10] where p_1 and p_2 are the distinct roots of the equation:

$$a_{11}p^4 - 2a_{16}p^3 + (2a_{12} + a_{66})p^2 - 2a_{26}p + a_{22} = 0 \quad (2)$$

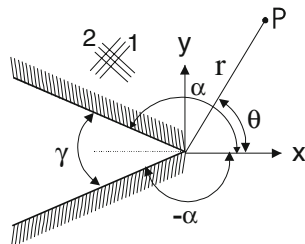
$$\begin{aligned} z_1 &= x + p_1y = r(\cos\theta + p_1 \sin\theta) \quad \text{and} \\ z_2 &= x + p_2y = r(\cos\theta + p_2 \sin\theta). \end{aligned} \quad (3)$$

For the free-free notch, displacement $\{u\}$ and stress function $\{\phi\}$ can be written as [11]:

$$\begin{Bmatrix} u \\ v \end{Bmatrix} = \left\{ [A][A]^{\delta+1}[B]^{-1} - [\bar{A}][\bar{A}]^{\delta+1}[\bar{B}]^{-1} \right\} \{g\} \quad (4)$$

$$\begin{Bmatrix} \phi_1 \\ \phi_2 \end{Bmatrix} = \left\{ [B][A]^{\delta+1}[B]^{-1} - [\bar{B}][\bar{A}]^{\delta+1}[\bar{B}]^{-1} \right\} \{g\} \quad (5)$$

Fig. 1 Geometry of a sharp V-notch. (The origin of interest is located at the notch tip and the center of the notch surface is in the negative x direction)



where \bar{x} means the conjugate of x , $\{g\}$ is a complex vector dependent on loading and the problem geometry, δ is an eigenvalue dependent on material properties and notch angle α (Fig. 1), $[A]$ and $[B]$ are Stroh matrices, [12, 13] and $[\Lambda]$ is dependent on z_1 , z_2 , and α , as follows (Wu and Chang 1993) [14]:

$$[A] = \begin{bmatrix} \frac{z_1}{\cos(-\alpha)+p_1 \sin(-\alpha)} & 0 \\ 0 & \frac{z_2}{\cos(-\alpha)+p_2 \sin(-\alpha)} \end{bmatrix} \quad (6)$$

Substituting equations (3) and (6) into equations (4) and (5) obtains:

$$\begin{Bmatrix} u \\ v \end{Bmatrix} = r^{\delta+1} \left\{ [A][\Gamma(\theta)]^{\delta+1}[B]^{-1} - [\bar{A}][\bar{\Gamma}(\theta)]^{\delta+1}[\bar{B}]^{-1} \right\} \{g\} \quad (7)$$

$$\begin{Bmatrix} \phi_1 \\ \phi_2 \end{Bmatrix} = r^{\delta+1} \left\{ [B][\Gamma(\theta)]^{\delta+1}[B]^{-1} - [\bar{B}][\bar{\Gamma}(\theta)]^{\delta+1}[\bar{B}]^{-1} \right\} \{g\} \quad (8)$$

where

$$[\Gamma(\theta)] = \begin{bmatrix} \frac{\cos\theta+p_1 \sin\theta}{\cos(-\alpha)+p_1 \sin(-\alpha)} & 0 \\ 0 & \frac{\cos\theta+p_2 \sin\theta}{\cos(-\alpha)+p_2 \sin(-\alpha)} \end{bmatrix} \quad (9)$$

For the free-free notch, $\{\phi\}$ should vanish at $\theta = \pm\alpha$. From equation (8), $\{\phi\}$ vanishes at $\theta = -\alpha$. When θ equals α , equation (8) changes to:

$$[K]\{g\} = \left\{ [B][\Gamma(\alpha)]^{\delta+1}[B]^{-1} - [\bar{B}][\bar{\Gamma}(\alpha)]^{\delta+1}[\bar{B}]^{-1} \right\} \{g\} = \{0\} \quad (10)$$

Thus, for a nontrivial solution of $\{g\}$, δ must be a root of $\det[K]=0$, which can be solved by Muller's method [15] to find the eigenvalues δ . The eigenvector $\{g\}$ of equation (10) can be obtained as follows:

$$\{g\} = \begin{Bmatrix} 1 \\ a \end{Bmatrix} g \quad (11)$$

where g is an unknown and a is obtained from equation (10). Equations (7) and (8) change to:

$$\begin{aligned} \begin{Bmatrix} u \\ v \end{Bmatrix} &= \begin{Bmatrix} U \\ V \end{Bmatrix} g = r^{\delta+1} \begin{Bmatrix} \hat{U} \\ \hat{V} \end{Bmatrix} g \quad \text{and} \\ \begin{Bmatrix} \phi_1 \\ \phi_2 \end{Bmatrix} &= \begin{Bmatrix} C \\ D \end{Bmatrix} g = r^{\delta+1} \begin{Bmatrix} \hat{C} \\ \hat{D} \end{Bmatrix} g \end{aligned} \quad (12)$$

where

$$\begin{Bmatrix} U \\ V \end{Bmatrix} = r^{\delta+1} \left\{ [A][\Gamma(\theta)]^{\delta+1}[B]^{-1} - [\bar{A}][\bar{\Gamma}(\alpha)]^{\delta+1}[\bar{B}]^{-1} \right\} \begin{Bmatrix} 1 \\ a \end{Bmatrix} \quad (13)$$

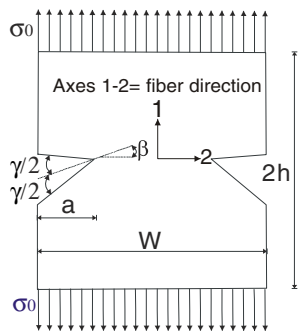


Fig. 2 Rectangular plates with double notches used in the experiments

$$\begin{Bmatrix} C \\ D \end{Bmatrix} = r^{\delta+1} \left\{ [B][\Gamma(\theta)]^{\delta+1}[B]^{-1} - [\bar{B}][\bar{\Gamma}(\theta)]^{\delta+1}[\bar{B}]^{-1} \right\} \begin{Bmatrix} 1 \\ a \end{Bmatrix} \quad (14)$$

In equation (12), g is the only unknown that is dependent on problem geometry and loading. For composite materials, we define the following four SIFs:

$$\sum_{j=1}^2 k_I(\delta_j) = \sum_{j=1}^2 \left(\sqrt{2\pi r}^{-\delta_j} \frac{\partial \phi_2}{\partial r} (r = \theta = 0) \right) \quad (15a)$$

$$\sum_{j=1}^2 k_{II}(\delta_j) = \sum_{j=1}^2 \left(\sqrt{2\pi r}^{-\delta_j} \frac{\partial \phi_1}{\partial r} (r = \theta = 0) \right) \quad (15b)$$

From equation (18), one obtains:

$$k_I(\delta_j) = \sqrt{2\pi} g_j [(\delta_j + 1)D / (r^{\delta_j+1})] (r = \theta = 0) \quad (15c)$$

$$k_{II}(\delta_j) = \sqrt{2\pi} g_j [(\delta_j + 1)C / (r^{\delta_j+1})] (r = \theta = 0) \quad (15d)$$

where $j=1$ or 2 .

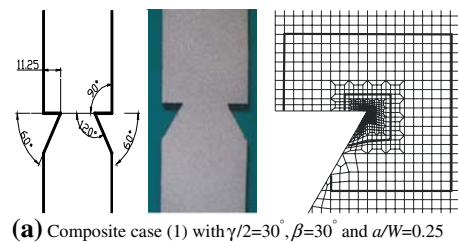
The physical meaning of $k_i(\delta_j)$ denotes the i th-mode SIF produced from the singularity of the j th eigenvalue. For a notch very near a crack, δ_1 and δ_2 will have similar values (near 0.5), so mode-1 and mode-2 SIFs can be combined as follows:

$$K_I = k_I(\delta_1) + k_I(\delta_2) \quad \text{and} \quad K_{II} = k_{II}(\delta_1) + k_{II}(\delta_2). \quad (16)$$

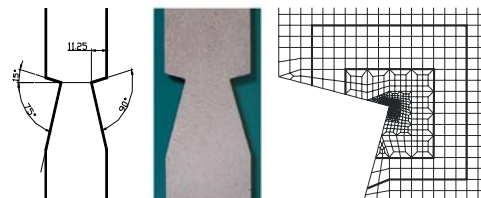
Image Correlation Experiments

Details of V-Notch Specimens

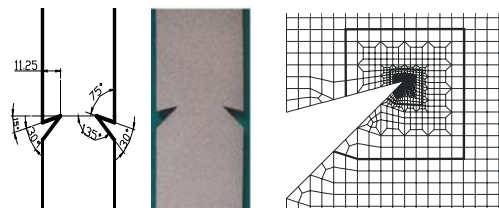
Experimental specimens contained three composite and two steel plates with double sharp V-notches (shown in Fig. 2) subjected to uniform tension σ_0 of 27 Mpa (applied force=3 kN) for composite plates and 185 Mpa (applied force=50 kN) for steel plates. The notch angle is γ , the angle between the notch centerline and the horizontal axis is β , and the specific notch length-to-plate width ratio is a/W . As shown in Fig. 3, the five specimens are: (1) a composite plate with $\gamma/2=30^\circ$ and $\beta=30^\circ$, (2) a composite



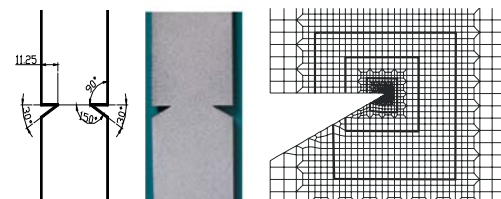
(a) Composite case (1) with $\gamma/2=30^\circ$, $\beta=30^\circ$ and $a/W=0.25$



(b) Composite case (2) with $\gamma/2=45^\circ$, $\beta=30^\circ$ and $a/W=0.25$



(c) Composite case (3) with $\gamma/2=15^\circ$, $\beta=30^\circ$ and $a/W=0.25$ (Steel plate case (4) has the same dimensions and finite element mesh as this specimen.)



(d) Steel case (5) with $\gamma/2=15^\circ$, $\beta=15^\circ$ and $a/W=0.25$

Fig. 3 Details of the dimensions and finite element mesh for the double notch specimen. **(a)** Composite case (1) with $\gamma/2=30^\circ$, $\beta=30^\circ$ and $a/W=0.25$. **(b)** Composite case (2) with $\gamma/2=45^\circ$, $\beta=30^\circ$ and $a/W=0.25$. **(c)** Composite case (3) with $\gamma/2=15^\circ$, $\beta=30^\circ$ and $a/W=0.25$ (Steel plate case (4) has the same dimensions and finite element mesh as this specimen). **(d)** Steel case (5) with $\gamma/2=15^\circ$, $\beta=15^\circ$ and $a/W=0.25$

Table 1 The 1st and 2nd eigenvalues ($\delta+1$) of the three experimental cases solved using Muller's method

Mode	Specimen 1	Specimen 2	Specimen 3	Specimen 4	Specimen 5
1	0.50941	0.53836	0.50104	0.50145	0.54448
2	0.69891	0.86922	0.58265	0.59819	0.90853

plate with $\gamma/2=45^\circ$ and $\beta=30^\circ$, (3) a composite plate with $\gamma/2=15^\circ$, $\beta=30^\circ$, (4) a steel plate with $\gamma/2=15^\circ$ and $\beta=30^\circ$, and (5) a steel plate with $\gamma/2=15^\circ$ and $\beta=15^\circ$. The ratio a/W for all the specimens is 0.25. The dimensions of the plates are 45 mm wide and 300 mm long. Plate thickness is 2.45 mm for composite plates and 6 mm for steel plates. The material properties are $E_{11}=70.24$ Gpa, $E_{22}=35.45$ Gpa, $G_{12}=11.4$ Gpa, and $\nu_{12}=0.246$ for composite plates and $E=225$ Gpa and $\nu=0.29$ for steel plates, as evaluated from strain-gauge experiments. The composite material is a 12 K-carbon-fiber/epoxy [0/0/45/90/-45/0/0/90/0/0/-45/90/45/0/0] with a yield stress of 150 Mpa, and the yield stress of steel specimens is 680 Mpa. The eigenvalues ($\delta+1$) of the three cases solved by Muller's method are listed in Table 1, in which the values only depend on the material properties and angle γ .

Optical System and Experimental Details

Similar to reference [16], the optical system (Fig. 4), which can take a picture of an actual area of 20 mm by 15 mm with $4,992 \times 3,328$ -pixel resolution, was controlled by camera shooting software, and a shutter speed of $1/250$ s, the f number of the camera aperture of 10, and an ISO of 100 were set. The Canon EOS 1D_S-MarkII digital camera with a Sigma lens (Macro 150 mm/2.8EX DG) and two rings of the Kenko extension tube sets (20 and 36 mm) was supported by a strong tripod. Two light sources were provided by four optical-fiber lights transferred from a 20 V to 150 W halogen lamp. To obtain pictures without distortion, the images were saved as uncompressed TIFF files. To apply

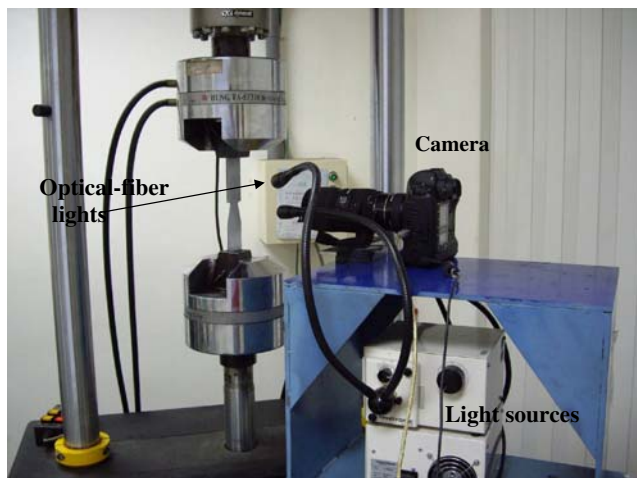


Fig. 4 Details of the optical system

the digital image correlation method, random patterns on the specimen surfaces are required (Fig. 3). This kind of pattern can be obtained by first painting the specimen surface with white paint, and then spraying it with a mist of black paint.

In the experiment, five specimens (Fig. 3) were tested using the 100-KN Instron-8800 servo-hydraulic testing machine under uniaxially tensile loads. First, the specimen was mounted and the optical system aimed at the measured zone. When the load was set to zero (un-deformed condition), a picture was taken for reference. The load was then increased to 3 kN for composite plates or 50 kN for steel plates and the next picture was taken (deformed condition). Due to micro-vibrations, the maximum error ($\text{Error}_{\text{pixel}}$) of pixels during taking a picture was defined as [16]: $\text{Error}_{\text{pixel}} = S_{\text{shutter}} V_{\text{vibration}} / P_{\text{scale}}$, where S_{shutter} ($=1/250$ s) is the camera shutter speed, $V_{\text{vibration}}$ (mm/s) is the maximum vibration velocity on the laboratory and P_{scale} ($=5.3E-3$ mm/pixel) is the picture resolution equal to the actual picture length over the pixels within the length. This error ($\text{Error}_{\text{pixel}}$) only contains that of laboratory micro-vibration, such as the vibration generated from the loading machine. Since the current experiments were set up without any vibration isolation scheme, it is reasonable to assume that the major error is generated from this term. During the experiments, three velocity meters were installed on the Instron machine to measure three-direction vibrations, and obtained the maximum $V_{\text{vibration}}$ of 0.08 mm/s. Thus, $\text{Error}_{\text{pixel}}$ equal to 0.06 pixels was the major inaccuracy in our experiments due to the laboratory micro-vibration.

Image-Correlation Method and Analysis Procedures

Two subsets are commonly compared using the cross-correlation coefficient, C , as follows [17]:

$$C\left(x, y, u, v, \frac{\partial u}{\partial x}, \frac{\partial u}{\partial y}, \frac{\partial v}{\partial x}, \frac{\partial v}{\partial y}\right) = \frac{\sum [f(x, y) \cdot g(x^*, y^*)]}{\left[\sum (f(x, y)^2) \cdot \sum (g(x^*, y^*)^2)\right]^{1/2}} \quad (17)$$

where $f(x, y)$ are undeformed subset intensity values at selected points within the subset, and $g(x^*, y^*)$ are deformed subset intensity values at selected points within the subset,

$$x^* = x + u + \frac{\partial u}{\partial x} \Delta x + \frac{\partial u}{\partial y} \Delta y \quad \text{and} \quad y^* = y + v + \frac{\partial v}{\partial x} \Delta x + \frac{\partial v}{\partial y} \Delta y \quad (18)$$

where x is the center point x -coordinate of the subset, y is the center point y -coordinate of the subset, u is the center point x -displacement, v is the center point y -displacement, $\frac{\partial u}{\partial x}$, $\frac{\partial u}{\partial y}$, $\frac{\partial v}{\partial x}$, $\frac{\partial v}{\partial y}$ are derivative terms at the center point, Δx is the chosen point x -direction distance from the center point, and Δy is the chosen point y -direction distance from the center point.

After the experiment, the undeformed and deformed TIFF files were processed by a PC-based program called CCD80 (<http://myweb.ncku.edu.tw/~juju>). This FORTRAN program uses the image-correlation method to find the displacements and strains at the centers of square blocks in the image.

Calculations of Stress and H-Integral Using Displacement Fields

Calculation and Smoothing of Displacements

Experimental errors in displacement often lead to inaccurate stress calculations; moreover, the H-integral requires boundary displacements that cannot be measured by the image correlation method. This study uses the Lagrange element to smooth internal displacements and to calculate boundary displacements as well. For the smoothing procedure, a nine-node Lagrange element is used. The external forces at the center node of the element should be zero if the body force is ignored. Thus, for each element containing displacements at eight points along the element boundary, one can calculate the displacements at the center point using this zero internal force condition, and then, shift one point to perform this procedure again. After all the points are looped a number of times (10 to 100 times), the unbalanced stresses on the domain will be small, and the displacement field will be smooth. This procedure to smooth linear elastic displacements is systematic and requires little computer time (under 1 second using a regular notebook).

A similar procedure is used to find the boundary displacements. The nodal forces $\{f_b\}$ inside a Lagrange element or along the traction-free boundary should be zero, so:

$$\{f_b\} = [K_f]\{u_{node}\} = \{0\} \quad (19)$$

where $[K_f]$ is the stiffness matrix for the nodes inside the element or along the traction-free boundary, and $\{u_{node}\}$ is the element nodal displacement vector.

For a point near or inside a Lagrange element, its displacements u_i can be interpolated using the element nodal displacement vector $\{u\}$ as follows:

$$u_i = [N_i]\{u_{node}\} \quad (20)$$

where $[N_i]$ is the shape function of the Lagrange element at this point; the displacement can be vertical or horizontal. For n points near or inside this element, the equation of the residue π can be obtained using equations (19) and (20).

$$\pi = \left(\sum_{i=1}^n [N_i]\{u_{node}\} - u_i \right)^2 + \{\lambda\}^T ([K_f]\{u_{node}\} - \{0\}) \quad (21)$$

where $\{\lambda\}$ is the Lagrange multiplier vector. To minimize the residue ($\partial\pi/\partial\{u_{node}\}=0$ and $\partial\pi/\partial\{\lambda\}=0$), one obtains:

$$\begin{bmatrix} \sum_{i=1}^n [N_i]^T [N_i] & [K_f]^T \\ [K_f] & 0 \end{bmatrix} \begin{Bmatrix} \{u_{node}\} \\ \{\lambda\} \end{Bmatrix} = \begin{Bmatrix} \sum_{i=1}^n [N_i]^T u_i \\ \{0\} \end{Bmatrix} \quad (22)$$

Equation (22) can be solved directly to find $\{u_{node}\}$ which includes the displacements along the boundary. Subsequently, the nodal displacements $\{u_{node}\}$ are used to calculate the stresses at the Gaussian points, and an extrapolation scheme is used to find the stresses on the element nodes. The above procedures do not require a mesh, but only a Lagrange element, to smooth internal displacements, calculate boundary displacements, and generate element stresses, so the use of this method is considerably simple. Moreover, since the equilibrium equation was used into the above procedures, this method is not only a smooth procedure but also a scheme to correct the displacements. All the finite element theory, such as the shape function and Lagrange element, used in this section can be found in reference [18].

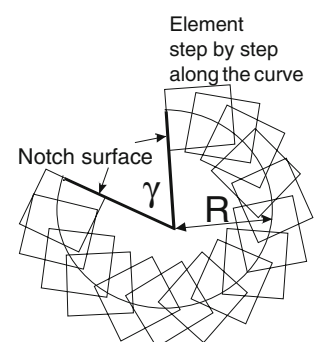
Calculation of the H-Integral

The H-integral is defined as follows [19]:

$$H = \int_{\Gamma} (\{u\}^T \{t_{com}\} - \{u_{com}\}^T \{t\}) ds \quad (23)$$

where $\{u\}$ and $\{t\}$ are the actual displacement and traction vectors, respectively, and $\{u_{com}\}$ and $\{t_{com}\}$ are comple-

Fig. 5 A loop with Lagrange elements along the curve for finding the H-integral



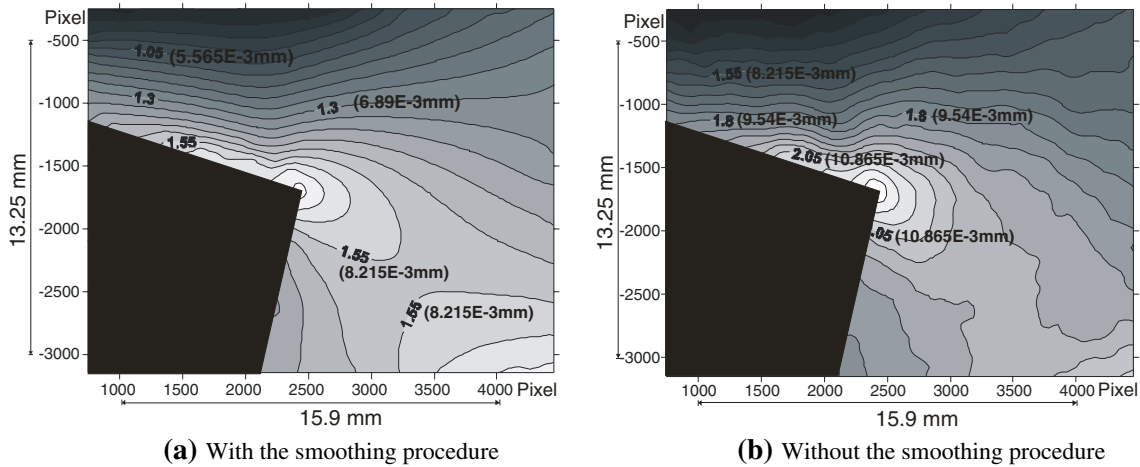


Fig. 6 Deformation contours and pictures from image-correlation experiments for specimens of case (2) ($\gamma/2=45^\circ$, $\beta=30^\circ$, $\sigma_0=27$ Mpa) (Unit=pixel, one pixel=5.3E-3 mm). **(a)** With the smoothing procedure. **(b)** Without the smoothing procedure

mentary displacement and traction vectors, respectively. Using equations (9) and (10) for the loop very near the notch tip, the H-integral is changed as follows:

$$H = \int_{-\alpha}^{\alpha} \left(\{u_{\delta=\delta_j}\}^T \partial \{ \phi_{\delta=\Delta_j} \} / \partial \theta - \{u_{\delta=\Delta_j}\}^T \partial \{ \phi_{\delta=\delta_j} \} / \partial \theta \right) d\theta \tag{24}$$

where $\delta = \delta_j$ or Δ_j means that a single eigenvalue of δ_j or Δ_j is substituted into equations (9) or (10) to find the displacement or stress function vector, and $\partial \{ \varphi \} / \partial \theta$ is the traction vector at angle θ . Let the complementary eigenvalue Δ_{j+1} equal $-(\delta_j+1)$, and substituting equation (19) into (24) for $r=0$, we obtain:

$$H = g \int_{-\alpha}^{\alpha} \text{Im} \left(\left[\hat{U}_{\delta=\delta_j} \quad \hat{V}_{\delta=\delta_j} \right] \begin{Bmatrix} \hat{C}l_{\delta=\Delta_j} \\ \hat{D}l_{\delta=\Delta_j} \end{Bmatrix} \right) - \left[\hat{U}_{\delta=\Delta_j} \quad \hat{V}_{\delta=\Delta_j} \right] \begin{Bmatrix} \hat{C}l_{\delta=\delta_j} \\ \hat{D}l_{\delta=\delta_j} \end{Bmatrix} \right) d\theta = g_j H^* \tag{25a}$$

where

$$\begin{Bmatrix} \hat{C}l_{\delta} \\ \hat{D}l_{\delta} \end{Bmatrix} = (\delta + 1) \left\{ [B][d\Gamma(\theta)/d\theta]^{\delta+1} [B]^{-1} - [\bar{B}][\overline{d\Gamma(\theta)/d\theta}]^{\delta+1} [\bar{B}]^{-1} \right\} \begin{Bmatrix} 1 \\ a \end{Bmatrix} \tag{25b}$$

$$[d\Gamma(\theta)/d\theta] = \begin{bmatrix} \frac{-\sin \theta + p_1 \cos \theta}{\cos(-\alpha) + p_1 \sin(-\alpha)} & 0 \\ 0 & \frac{-\sin \theta + p_2 \cos \theta}{\cos(-\alpha) + p_2 \sin(-\alpha)} \end{bmatrix} \tag{25c}$$

When the notch angle α and material properties are known, the integral H^* of equation (25a) can be obtained directly using the Simpson integration method, which means that H^* only depends on α and the material properties and is independent of experimental or finite element results. The displacements ($\{u\}$) and tractions ($\{t\}$) from the experiment using the procedures in the section “Calculation and Smoothing of Displacements” are substituted into equation (23) to find the H-integral. The

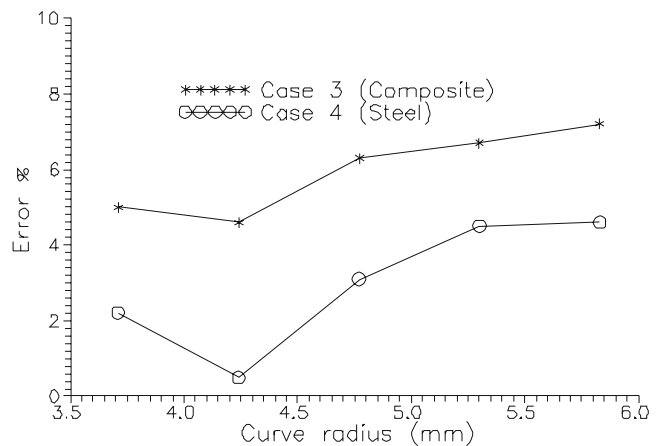


Fig. 7 The experimental error of H-integrals changing with the curve radius of loops

Table 2 Mixed-mode SIFs for double sharp-V notches using the H-integral method with plane stress finite element analysis with 8-node isoparametric elements (SIFs are averaged from the three loops, as shown in Fig. 3.)

case	$\gamma/2$	β	H-integral method and FEM			
			$F_I(\delta_1)$	$F_{II}(\delta_1)$	$F_I(\delta_2)$	$F_{II}(\delta_2)$
1 (composite)	30°	30°	1.01407	0.14675	0.000546	0.42229
2 (composite)	45°	30°	1.07860	0.15300	0.049871	0.55022
3 (composite)	15°	30°	0.99087	0.13710	0.001661	0.33393
4 (steel)	15°	30°	1.0286	0	0	0.45041
5 (steel)	15°	15°	1.1429	0	0	0.25544

complementary eigenvalue can be chosen as $\Delta_j+1 = -(\delta_j+1)$ for $j=1$ or 2 to evaluate $\{u_{com}\}$ and $\{t_{com}\}$. The tractions are calculated as follows:

$$\{t\} = [\sigma]\{n\} \tag{26}$$

where $[\sigma]$ is the stress tensor and $\{n\}$ is the normal direction at the point of the integration loop. It is noted that the stress and displacement fields and the complementary solution should be under the notch x–y coordinates, as shown in Fig. 1. Using the above procedure, one can evaluate the H-integral from finite element results without difficulty, and three loops as shown in Fig. 3 were used to find the averaged H-integral, which was compared with that calculated from the image correlation experiments.

The displacement vector $\{u\}$ of equation (23) at the notch tip is defined to be zero. In the finite element analysis, the displacements of other locations need to eliminate the notch-tip displacements. However, they are unknown in the experiment, so a displacement shift is used in equation (23) as follows:

$$H_{exp} = \int_{\Gamma} \left((\{u\} - \{u_{tip}\})^T \{t_{com}\} - \{u_{com}\}^T \{t\} \right) ds \tag{27}$$

where $\{u_{tip}\}$ is the actual displacement at the notch tip. Let $\{u_{tip}\} = \begin{Bmatrix} u_{xtip} \\ u_{ytip} \end{Bmatrix}$ and $\{t_{com}\} = \begin{Bmatrix} t_{xcom} \\ t_{ycom} \end{Bmatrix}$, and then equation (31) changes to:

$$H = H_{exp} + T_x u_{xtip} + T_y u_{ytip} = [1T_x T_y] [H_{exp} u_{xtip} u_{ytip}]^T = [K_T] \{H_u\} \tag{28}$$

Table 3 Errors of mixed-mode SIFs for anisotropic double sharp-V notches using the H-integral method from image correlation experiments (SIFs are calculated from nine loops with the loop radius from 2.65 mm to 6.89 mm.)

Experiment	Illustration			$F_I(\delta_1)$	$F_{II}(\delta_1)$	$F_I(\delta_2)$	$F_{II}(\delta_2)$	Error%
	$\gamma/2$	β	a/W					
Case 1 (Composite)	30°	30°	0.25	1.12682	0.16306	0.00059	0.41930	8.3
Case 2 (Composite)	45°	30°	0.25	1.02914	0.14678	0.05050	0.62238	7.0
Case 3 (Composite)	15°	30°	0.25	1.04665	0.14460	0.00160	0.33860	4.6
Case 4 (Steel)	15°	30°	0.25	1.00351	0	0	0.45343	2.0
Case 5 (Steel)	15°	15°	0.25	1.14421	0	0	0.30737	3.8

where $T_x = \int_{\Gamma} t_{xcom} ds$ and $T_y = \int_{\Gamma} t_{ycom} ds$. There are three unknowns, H_{exp} , u_{xtip} , and u_{ytip} , in equation (28), and one can select more than one loop incorporating the least-squares method to find the three unknowns. The least-squares equation is as follows:

$$\left(\sum [K_T]^T [K_T] \right) \{H_u\} = \sum [K_T]^T H \tag{29}$$

Finally, g_j in equation (25a) is equal to H_{exp}/H^* , and the SIFs are computed using equations (15c) and (15d). Equation (29) can obtain the average H-integral from a number of loops. In this study, the loop is set along an arch with the inputted radius as shown in Fig. 5. The center of the Lagrange element mentioned in the section “Calculation and Smoothing of Displacements” is located on this curve so that the displacements and stresses can be found. The element is shifted step by step along the curve to obtain the displacement and stress fields for the H-integral calculation.

The size of the Lagrange element should be sufficiently large to include enough displacement data for equation (22). In this study, we used a five-by-five-node Lagrange element (25 nodes), and the element size was set to include about 50 displacement points.

Experimental Results and Comparisons

In this section, the H-integral obtained from the finite element analysis is used to validate the SIFs calculated from image correlation experiments. The finite element program from reference [20] was used with 8-node



isoparametric elements in the linear-elastic analysis. The notch tip position was set at the intersection point of the two notch surface, which is easy to obtain using computer software such as Microsoft Paint. The dimensionless SIFs are defined as:

$$F_I(\delta_j) = \frac{k_I(\delta_j)}{\sigma_0 \sqrt{\pi a^{-\delta_j}}} \quad \text{and} \quad F_{II}(\delta_j) = \frac{k_{II}(\delta_j)}{\sigma_0 \sqrt{\pi a^{-\delta_j}}} \quad \text{for } j = 1, 2 \quad (30)$$

where σ_0 is the far-field applied normal stress and a (11.25 mm) is the specimen notch length. The error of the current least-squares method is defined as:

$$\text{Error} = \frac{\sum_{i=I,II} (|F_i^{FEM}(\delta_1) - F_i^{EXP}(\delta_1)| + |F_i^{FEM}(\delta_2) - F_i^{EXP}(\delta_2)|)}{\sum_{i=I,II} (|F_i^{FEM}(\delta_1)| + |F_i^{FEM}(\delta_2)|)} \quad (31)$$

where $F_i^{FEM}(\delta_j)$ are the SIFs of F_I and F_{II} obtained from the finite element analyses and $F_i^{EXP}(\delta_j)$ are the SIFs calculated from the image correlation experiments.

The correlation coefficient [equation (17)] of the five experiments is from 0.9970 to 0.9999, and the average value is about 0.9998. Figure 6 shows the vertical deformation contour of specimen 2 from the image-correlation experiment before and after using the proposed smoothing scheme. These figures show that the deformation noise can be considerably decreased using the smoothing scheme. In the H-integral calculation, the curve radius of the loop was set to 2.65 mm (500 pixels) to 6.89 mm (1300 pixels) with an interval of 0.53 mm (100 pixels), and there were nine loops in total. First, we used five loops in equation (29) to find H_{exp} and SIFs for specimens 3 and 4, which are shown in Fig. 7. This figure indicates that although the errors slightly vary with the loop radius, they are not large. The error for the anisotropic specimen is larger than that for the isotropic specimen, which is due the former's complex material properties. The error gradually increases with increasing loop radius, because the reason that the region far away from the notch tip has smaller stress, which is easily influenced by experimental error. Moreover, the loop close to the notch tip may also have large error because the stress field near the notch tip is singular.

All nine loops were used in equation (29) to find the SIFs of the five specimens, which means that the SIFs are the average of the nine loops. Table 2 shows the H-integral results from finite element analyses and Table 3 shows those from image correlation experiments. The maximum SIF error of the image-correlation experiment is about 8%, which should be acceptable for mixed-mode fracture problems of a sharp V-notch.

Conclusion

This study developed an H-integral scheme to calculate the notch SIFs using the displacement fields of image-correlation experiments. A nine-node Lagrange element based on the weak form of the equilibrium equation was used to smooth the displacements inside the domain; moreover, a 25-node Lagrange element was used to interpolate or extrapolate the experimental displacements into element nodes and specimen boundaries. Since the H-integral requires displacements at the notch tip that cannot be found in the experiment, notch-tip displacements were set as unknowns and the least-squares method was applied to find them and the H-integral. The hardware of the image system contains only a digital camera with a regular macro lens that is easy to obtain in the commercial market. Moreover, the proposed smoothing procedure of the image correlation method is simple and systematic. Compared with the SIFs calculated from finite element method, the proposed experimental method can be used to accurately calculate the SIFs of a sharp V-notch.

References

- Della-Ventura D, Smith RNL (1998) Some applications of singular fields in the solution of crack problems. *Int J Numer Methods Eng* 42:927–942
- Potti PKG, Rao BN, Srivastava VK (2001) Fracture strength of composite laminates containing surface notches. *Adv Compos Mater* 10:29–37
- Niu LS, Shi HJ, Robin C, Pluvinage G (2001) Elastic and elastic-plastic fields on circular rings containing a v-notch under inclined loads. *Eng Fract Mech* 68:949–962
- Kondo T, Kobayashi M, Sekine H (2001) Strain gage method for determining stress intensities of sharp-notched strips. *Exp Mech* 41:1–7
- Mattoni MA, Zok FW (2003) A method for determining the stress intensity factor of a single edge-notched tensile specimen. *Int J Fract* 119:376–392
- Kumagai S, Shindo Y (2004) Experimental and analytical evaluation of the notched tensile fracture of CFRP-woven laminates at low temperatures. *J Compos Mater* 38:1151–1164
- Xu W, Yao XF, Xu MQ, Jin GC, Yeh HY (2004) Fracture characterizations of V-notch tip in PMMA polymer material. *Polym Test* 23:509–515
- El-Hajjar R, Haj-Ali R (2005) Mode-I fracture toughness testing of thick section FRP composites using the ESE(T) specimen. *Eng Fract Mech* 72:631–643
- Yao XF, Yeh HY, Xu W (2006) Fracture investigation at V-notch tip using coherent gradient sensing (CGS). *Int J Solids Struct* 43:1189–1200
- Lekhnitskii SG (1963) *Theory of elasticity of an anisotropic body*. Holden-Day, San Francisco
- Ting TCT (1996) *Anisotropic elasticity: theory and application*. Oxford University Press, New York
- Stroh AN (1962) Steady state problems in anisotropic elasticity. *J Math Phys* 41:77–103

13. Ting TCT (1992) Barnett-Lothe tensors and their associated tensors for monoclinic materials with the symmetry plane at $x_3=0$. *J Elast* 27:143–165
14. Wu K-C, Chang F-T (1993) Near-tip field in a notched body with dislocations and body forces. *ASME J Appl Mech* 60:936–941
15. Press WH, Flannery BP, Teukolsky SA, Vetterling WT (1986) *Numerical recipes, the art of scientific computing*. Cambridge University Press, New York
16. Ju SH, Liu SH (2007) Determining stress intensity factors of composites using crack opening displacement. *Compos Struct* 81:614–621
17. Bruck HA, McNeill SR, Sutton MA, Peters WH (1989) Digital image correlation using Newton-Raphson method of partial differential correlation. *Exp Mech* 29:261–267
18. Cook RD, Malkus DS, Plesha ME (1989) *Concepts and applications of finite element analysis*, 3rd edn. Wiley, New York
19. Labossiere PEW, Dunn ML (1998) Calculation of stress intensities at sharp notches in anisotropic media. *Eng Fract Mech* 61:635–654
20. Ju SH (1997) Development a nonlinear finite element program with rigid link and contact element. NSC-86-2213-E-006-063, This report and source codes in an executable compressed file `nfemnew.exe` of MS-Windows can be obtained from the internet myweb@mail.ncku.edu.tw/~juju